Micromechanical measurement of beating patterns in the quantum oscillatory chemical potential of InGaAs quantum wells due to spin-orbit coupling

Florian Herzog, Christian Heyn, Hilde Hardtdegen, Thomas Schäpers, Marc A. Wilde, and Dirk Grundler

Citation: Applied Physics Letters **107**, 092101 (2015); doi: 10.1063/1.4929840
View online: http://dx.doi.org/10.1063/1.4929840
View Table of Contents: http://scitation.aip.org/content/aip/journal/apl/107/9?ver=pdfcov
Published by the AIP Publishing

Micromechanical measurement of beating patterns in the quantum oscillatory chemical potential of InGaAs quantum wells due to spin-orbit coupling

Florian Herzog,[1,a)] Christian Heyn,[2] Hilde Hardtdegen,[3] Thomas Schäpers,[3] Marc A. Wilde,[1,b)] and Dirk Grundler[1,4]
[1]*Lehrstuhl für Physik funktionaler Schichtsysteme, Physik Department, Technische Universität München, James-Franck-Strasse 1, D-85748 Garching b. München, Germany*
[2]*Institut für Nanostruktur- und Festkörperphysik, Universität Hamburg, Jungiusstr. 11, D-20355 Hamburg, Germany*
[3]*Peter Grünberg Institut (PGI-9) and JARA-FIT Jülich-Aachen Research Alliance, Forschungszentrum Jülich, D-52425 Jülich, Germany*
[4]*Laboratory of Nanoscale Magnetic Materials and Magnonics (LMGN), Institute of Materials, École Polytechnique Fédérale de Lausanne, CH-1015 Lausanne, Switzerland*

(Received 3 July 2015; accepted 19 August 2015; published online 31 August 2015)

The quantum oscillatory magnetization $M(B)$ and chemical potential $\mu(B)$ of a two-dimensional (2D) electron system provide important and complementary information about its ground state energy at low temperature T. We developed a technique that provides both quantities in the same cool-down process via a decoupled static operation and resonant excitation of a micromechanical cantilever. On InGaAs/InP heterostructures, we observed beating patterns in both $M(B)$ and $\mu(B)$ attributed to spin-orbit interaction. A significantly enhanced sensitivity in μ enabled us to extract Rashba and Dresselhaus parameters with high accuracy. The technique is powerful for detailed investigations on the electronic properties of 2D materials. © *2015 AIP Publishing LLC*.
[http://dx.doi.org/10.1063/1.4929840]

Thermodynamic quantities such as the magnetization M and chemical potential μ are of great potential to investigate the ground state properties of two-dimensional electron systems (2DESs).[1,2] They enable insights into energy spectra and the density of states (DOS) in a magnetic field B and can be compared directly to theoretical calculations based on a specific model Hamiltonian. However, accessing M and μ experimentally turned out to be challenging. Measurements of quantum oscillations of M in 2DESs were performed with SQUID[3,4] or torque magnetometers.[1,2,5] Operated in a quasi-static mode, the latter techniques measured the static magnetic torque $\tau = \mathbf{M} \times \mathbf{B}$ and featured a high sensitivity that scaled linearly with the magnetic field $\mathbf{B}$. The resonant excitation of mechanical modes of microcantilevers was reported to further enhance the sensitivity in M.[6–8] The quasi-statically detected quantum oscillatory magnetization $M(B)$, i.e., the de Haas-van Alphen (dHvA) effect, was shown to exhibit beating patterns when the 2DESs exhibited spin-orbit interaction (SOI).[9] However, in AlGaAs-based systems, it was possible to detect beatings only at high tilt angles of B,[10] and in asymmetric InGaAs quantum wells (QWs) only a single beat node was resolved at low tilt angles due to the inherently small sensitivity of torque magnetometry at small B.[11] The chemical potential μ of a 2DES was detected in separate experiments using nanostructured single electron transistors,[12] or via magnetocapacitance measurements[13] and electrometry on bilayer 2DESs[14,15] that were formed in dedicated heterostructures. State-of-the-art measurements of μ revealed signatures of Wigner crystal formation in bilayered 2DESs[16] and of quantum Hall ferromagnetism in bilayer graphene.[17,18] Still, SOI phenomena in quantum oscillations of μ lack detailed experimental investigations. SOI originates from bulk and structural inversion asymmetries in zinc-blende heterostructures. The interplay of corresponding Dresselhaus (D) and Rashba (R) contributions, respectively, is not universal. It rules the functionality and depends decisively on the design of a specific heterostructure.[19] While samples with a dominant R-term are suitable for gate-controlled spin manipulation,[20] devices with equal R and D terms could be used for effective spin filtering.[21]

In this letter, we present a micromechanical cantilever setup that allowed us to access $\mu(B)$ and $M(B)$ on one-and-the-same 2DES in the same cool-down process. We show how $\mu(B)$ is extracted from resonant gate voltage modulation applied to an InGaAs/InP heterostructure that exhibits SOI. We resolve quantum oscillatory behavior of μ including two nodes of the SOI-induced beating pattern. Applying a single-particle model Hamiltonian, we find that both a dominant R term as well as a small D term are required to model $\mu(B)$. The combined and simultaneous detection of μ and M as presented here is, in particular, interesting for studies on quantum Hall ferromagnetism for which $\mu(B)$ has been reported, but a direct measurement of the magnetic hysteresis $M(B)$ has not yet been accomplished. The integrated field-effect electrode is relevant when the gate-controlled interplay of D- and R-SOI[22,23] is to be studied in $\mu(B)$. The technique is also of great potential for investigations on electronic properties of 2D materials.[24]

Rectangular mesas were etched from modulation-doped 10 nm-thick asymmetric $In_{0.77}Ga_{0.23}As$ QWs grown on (001)-oriented InP substrates by metal-organic vapor phase

a)Electronic mail: Florian.Herzog@ph.tum.de
b)Electronic mail: mwilde@ph.tum.de

epitaxy [inset of Fig. 2(b)]. The QWs were strained and optimized for, both, high electron mobility and dominant R-SOI.[25] Four diffused AuGe contacts and an Au top gate electrode were integrated. The samples were thinned down to $\approx 10\,\mu$m to reduce their weight and then placed on specially tailored GaAs cantilevers in flip-chip technique [Figs. 1(a) and 1(b)].[26,27] These cantilevers contained a thin-film coil used for calibration and Au leads on their top surface to contact the 2DES [Fig. 1(b)]. The magnetization $\mathbf{M}$ of the 2DES caused by the in-plane orbital motion of the electrons is perpendicular to the sample surface. A magnetic field $\mathbf{B}$ applied at an angle α with respect to $\mathbf{M}$ causes a torque $\tau = \mathbf{M} \times \mathbf{B}$ and deflects the paddle from its zero-field position. We read out the deflection with a fiber optics interferometer at a laser wavelength of 1310 nm. The characteristic interference pattern measured by a photo voltage U_{PD} is sketched in Fig. 1(c). Calibration of the setup is carried out by applying a current I through the thin-film coil on the cantilever, generating a well-defined magnetic moment $m = IA_c$ (A_c is the area surrounded by the coil).

For quasi-static measurements of M, we adjust the vertical fiber position by means of a piezoceramic tube in a closed feedback loop in order to maintain a constant distance d. The point of operation is chosen to be one of the inflection points of the interference pattern $U_{\mathrm{PD}}(d)$. The static deflection of the cantilever is measured via the applied voltage at the piezoceramic tube U_{piezo}. In addition to the static measurement, we apply an oscillating gate voltage $U_g = U_{g,0} + \delta U_g \sin \omega t$, which leads to a *dynamic* modulation of both the electron number with amplitude $\delta N = A_m(\partial n_{2D}/\partial U_g)\,\delta U_g$ (A_m is the total mesa area) and the magnetization $\delta M = (\partial M/\partial N)\delta N$, where $N = n_{2D} \times A_m$. The transfer function $\partial n_{2D}/\partial U_g$ is extracted from static measurements of the electron density n_{2D} as a function of the applied gate voltage U_g. The modulation of M is performed at an oscillation frequency $f = \omega/(2\pi)$ slightly smaller than the resonance frequency of the cantilever and leads to a periodic deflection of the cantilever with amplitude δd. Using standard lock-in technique, we measure δd via the amplitude of the oscillating photo voltage U_{PD} as sketched in Fig. 1(c). Low-pass filtering of the static feedback loop is used to decouple the static and dynamic measurements. The dynamic magnetization is derived as $\partial M/\partial N \approx \delta M/(\delta n_{2D} A_m)$. We emphasize that both quantities, M and $\partial M/\partial N$, are measured *simultaneously* as a function of the external applied field B in our approach. This allows for a direct comparison of M and μ. Different from the techniques used in Refs. 6 and 8, we address the 2DES properties by modulation of n_{2D} in the chemical-potential measurements such that the measured signal is not superimposed by background signals stemming from the substrate or the cantilever itself. Measurements were carried out inside a ^{3}He cryostat at a sample temperature of $T = 0.6$ K. The external field B was applied using a 2D vector magnet with a radial field strength of 4.5 T, which allowed for a continuous variation of α defined in Fig. 1.

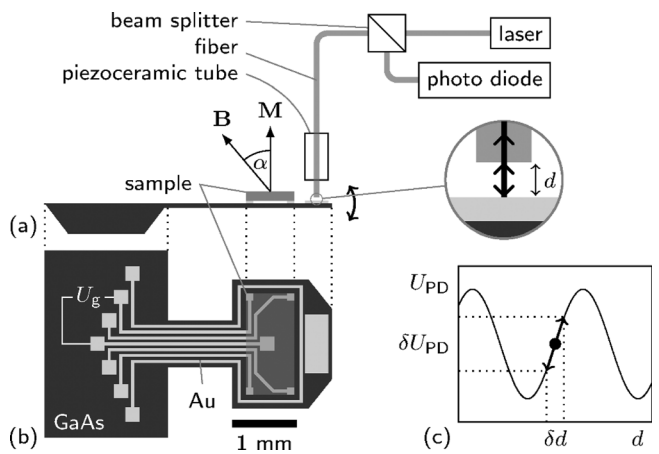

FIG. 1. (a) Schematic side-view of the cantilever with a mounted sample. The change in d due to the torque $\tau = \mathbf{M} \times \mathbf{B}$ is read out by means of an interferometer which forms between the cleaved edge of an optical fiber and the cantilever (see enlarged sketch). (b) Top view of the cantilever with electrical contacts and calibration coil. (c) Schematic photodiode voltage U_{PD} as a function of d. The working point for static operation as well as the response δU_{PD} in case of a cantilever oscillation with amplitude δd is indicated.

For analyzing the data, we access the chemical potential μ via the Maxwell relation $-(\partial \mathbf{M}/\partial N)_T = (\partial \mu/\partial \mathbf{B})_N$. μ is then obtained via

$$\mu = -\int \left(\frac{\partial \mathbf{M}}{\partial N}\right)_T \cdot d\mathbf{B}. \tag{1}$$

We model $M(B)$ and $\mu(B)$ by a fully quantum mechanical approach including SOI contributions. For this, we assume a 2DES subjected to $\mathbf{B}$ at an angle α with respect to its surface normal. The problem is formulated via the Hamiltonian $H = H_0 + H_R + H_D$ with the R-SOI term $H_R = \frac{\alpha_R}{\hbar}(\sigma_x \pi_y - \sigma_y \pi_x)$ and the D-SOI term $H_D = \frac{\beta_D}{\hbar}(\sigma_x \pi_x - \sigma_y \pi_y)$ being linear in wave vector k. Here, $H_0 = \frac{\pi^2}{2m^*} + g^* \mu_B \boldsymbol{\sigma} \cdot \mathbf{B}$ denotes the unperturbed Hamiltonian with Landau and Zeeman splitting ($\boldsymbol{\pi} = -i\hbar\nabla + e\mathbf{A}$ is the kinetic momentum with $\mathbf{B} = \nabla \times \mathbf{A}$, m^* is the effective mass, $\boldsymbol{\sigma} = (\sigma_x, \sigma_y, \sigma_z)$ is the vector of the Pauli spin matrices, $\hbar = h/(2\pi)$ is the reduced Planck constant, and α_R, β_D denote the R and D constants). Following Ref. 28, we diagonalize H in terms of eigenstates $|n, \pm\rangle$ of H_0 up to a finite $n_{\max}$ and extract the eigenvalues $E_{n'}(B)$ of H. Assuming a Gaussian level broadening $\Gamma \propto \sqrt{B_\perp}$ and applying Fermi-Dirac statistics, we calculate $\mu(B)$ and the total free energy $F(B)$ and derive the magnetization $M = -\partial F/\partial B$, as described in detail in Ref. 2. Here, we report on results obtained on two different samples named #4069-5B and #4069-5C that we prepared from the same heterostructure that was used in Ref. 11.

The light curves in Figs. 2(a) and 2(b) present simultaneous measurements of M and $\partial M/\partial N$ as a function of the perpendicular field $B_\perp = B \cos\alpha$ of sample #4069-5B, which was recorded at $\alpha = 39.0°$. M exhibits $1/B_\perp$-periodic dHvA oscillations. A background of interconnected splines, which varied slowly on the scale of the oscillation period, was subtracted from the raw M data in order to extract its oscillatory part. From the period in $1/B_\perp$, we extracted the electron density $n_{2D} = 8.57 \times 10^{11}\,\mathrm{cm}^{-2}$. The maximum visible filling factor $\nu = (hn_{2D})/(eB_\perp)$ was $\nu = 109$. A single beat node was identified at $B = 0.63$ T. For field values $B < 0.33$ T, the magnetic signal of the 2DES is found to be below the noise level.

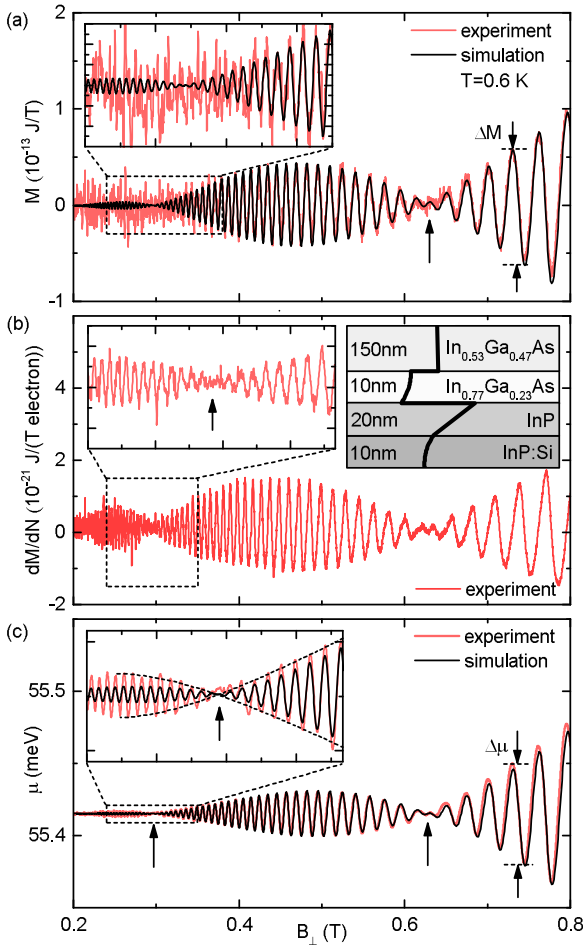

FIG. 2. Experimental traces (light curves) of (a) magnetization M, (b) dynamic magnetization $\partial M/\partial N$, and (c) chemical potential μ as a function of $B_\perp$. The curve in (c) derived from experimental data was offset by the theoretical zero-field Fermi energy $E_F = (\pi\hbar^2 n_{2D})/m^*$. The amplitudes ΔM and $\Delta\mu$ are indicated exemplarily for $\nu = 48$. The left insets show blow-ups of the second beat node. Fits of the envelopes were used to extract node positions [inset in (c)]. Model curves for $M(B)$ and $\mu(B)$ (black) were calculated using one and the same parameter set: $n_{2D} = 8.57 \times 10^{11}\,\mathrm{cm}^{-2}$, $m^* = 0.037 m_0$, $g^* = -4.45$, $\alpha_R = 4.44 \times 10^{-12}\,\mathrm{eVm}$, $\beta_D = 0.46 \times 10^{-12}\,\mathrm{eVm}$, $T = 0.6\,\mathrm{K}$, and $\Gamma = 0.83\,\mathrm{meV}/\sqrt{\mathrm{T}}$. The layer sequence and sketched conduction band edge[29] (thick line) are shown in the right inset of (b).

The oscillations in the dynamic magnetization $\partial M/\partial N$ were phase-shifted by a quarter of a period with respect to the dHvA oscillations. We applied $\Delta U_g = 5.6\,\mathrm{mV}$ at $f = 92\,\mathrm{Hz}$, corresponding to $\Delta n_{2D} = 0.015 \times 10^{11}\,\mathrm{cm}^{-2}$. This value was chosen such that the modulation amplitude in terms of the filling factor $\Delta\nu$ was smaller than 0.5, i.e., $\Delta n_{2D} < 0.5(eB_\perp)/h$ at $B_\perp \geq 0.21\,\mathrm{T}$. For this dynamic measurement, oscillations were detected down to 0.21 T corresponding to $\nu = 168$. The technique allowed us to resolve a second beat node at $B_\perp = 0.3\,\mathrm{T}$ [see inset of Fig. 2(b)]. Using Eq. (1), we then determined the oscillatory part of μ from the experimental data $\partial M/\partial N$ [light curve in Fig. 2(c)]. We shifted the curve by the zero-field Fermi energy given by $E_F = (\pi\hbar^2 n_{2D})/m^*$. We determined the field positions of the two beat nodes in $\mu(B)$ by fitting envelope functions based on low-order polynomials and finding their crossing points as sketched in the inset of Fig. 2(c). The corresponding field values exhibit error bars of 4 mT for the first and 3 mT for the second nodes.

In our model calculations, we searched for values of the field B at which $(E_{n'} - E_{n'-1}) = (E_{n'+1} - E_{n'})$, i.e., subsequent gaps of the energy levels were equal in size, and identified them as the theoretically predicted node positions. We then applied a fit routine to adjust the SOI parameters α_R and β_D until the calculated node positions matched the experimentally observed ones. For the remaining calculation parameters, we used $g^* = -4.45$ and $m^* = 0.037$.[11] For the modeling, we assumed that α_R was dominant, as was previously reported for the heterostructure.[30] Table I summarizes the results of the fitting for three different tilt angles α. The analysis yields a Dresselhaus contribution β_D that is smaller than α_R (by a factor of 10). The given error bars reflect the uncertainties in the node positions. Data analysis of sample #4069-5C provides consistent results for α_R and β_D.

Furthermore, we simulated the curves for M and μ by the model Hamiltonian introduced above using the parameters found for α_R and β_D in the previous fitting routine [black curves in Fig. 2(c)]. The only free parameter that we adjusted in the calculations was the level broadening of $\Gamma = 0.83\,\mathrm{meV}/\sqrt{\mathrm{T}}$ to match the amplitudes in the experiment. We stress that both model curves were obtained by using *one and the same* parameter set. Note that the node positions as well as the amplitude and shape of the oscillations of both experimental curves are reproduced quantitatively by the model calculations, except for the oscillation amplitude $\Delta\mu$ at small fields. This discrepancy between theoretical and experimental traces $\mu(B)$ is attributed to residual inhomogeneities across the wafer. It was not observed for sample #4069-5C, where a smaller broadening parameter of $\Gamma = 0.6\,\mathrm{meV}/\sqrt{\mathrm{T}}$ was used in the modeling (not shown). In $M(B)$, we were not able to resolve the second beat node predicted by the modeling [inset of Fig. 2(a)]. The noise level at small $B_\perp$ was too large.

In the following, we discuss our findings and their implications. The presented measurement technique both enabled simultaneous access to the thermodynamic quantities M and μ and offered an enhanced sensitivity for the dynamic measurement of μ. The enhanced sensitivity was attributed to an increased amplitude δd as the modulation frequency was close to the mechanical resonance frequency of the cantilever. δd was larger by a factor of $\approx$15 compared to the quasi-static operation.

The beat nodes in $\mu(B)$ allowed us to determine R- and D-SOI constants. We found $\beta_D \approx 0.1\alpha_R$ (β_D was measured with an accuracy of 20%). Model curves $\mu(B)$ deviated from the experimental data if only R-SOI was taken into account (not shown), as suggested by sole magnetization measurements on samples prepared from the same wafer.[11] Our combined experiments now show that both contributions are

TABLE I. Field positions of the first two beat nodes at different tilt angles α measured for sample #4069-5B and extracted SOI-constants α_R, β_D. For the calculation, we used $g^* = -4.45$, $m^* = 0.037 m_0$, and $n_{2D} = 8.57 \times 10^{11}\,\mathrm{cm}^{-2}$.

α (deg)	Node 1 (T)	Node 2 (T)	α_R (10^{-12} eV m)	β_D (10^{-12} eV m)
14.0	0.629	0.296	4.42 ± 0.02	0.48 ± 0.10
29.0	0.629	0.297	4.44 ± 0.02	0.43 ± 0.10
39.0	0.629	0.297	4.44 ± 0.02	0.46 ± 0.10

relevant and to be considered when aiming at spin-manipulation based on similar structures. For a perpendicular field orientation, the energy spectrum $E_{n'}(B)$ *does not depend* on the signs of α_R and β_D.[31] This holds true for increasing tilt angle α as long as the nodes do not shift to higher field values. This condition is fulfilled in Table I. Following this, we report absolute values of the SOI constants. A determination of the relative sign of α_R/β_D by magnetometry would require an experiment performed at large α as a function of φ.[32]

$M(B)$ and $\mu(B)$ detected by our setup provide complementary insights into the 2DES's ground state. $M = -\partial F/\partial B$ probes changes in the free energy F, while $\mu = \partial F/\partial N$ monitors the evolution of the highest occupied states. μ is not sensitive to changes in the low-lying energy states. In a single particle picture, the amplitudes of the quantum oscillations ΔM and $\Delta\mu$ are predicted to obey the relation $\Delta M/N = \Delta\mu/B$.[1] This was shown theoretically to hold true also for interacting electrons in the Hartree-Fock approximation.[33] For the data presented here, we experimentally confirm the validity of this relation (cf. Fig. 2). However, if dynamic screening is relevant, the relation $\Delta M/N = \Delta\mu/B$ is predicted to become invalid, and a strong enhancement of ΔM over $\Delta\mu$ is expected.[4] Our technique allows to explore this discrepancy experimentally.

In conclusion, we presented the simultaneous determination of magnetization $M(B)$ and chemical potential $\mu(B)$ of a 2DES using quasi-static and gate-modulated torque magnetometry. We reported beating patterns in both M and μ caused by spin-orbit interaction. The measurement technique presented here provides a powerful tool for detailed studies on electronic properties of low-dimensional electron systems in semiconductor heterostructures and 2D materials.

We gratefully acknowledge financial support by the DFG via SPP1285 (Grant No. GR1640/3), SPP1459 (Grant No. WI3320/1), and TRR80.

[1]S. A. J. Wiegers, M. Specht, L. P. Lévy, M. Y. Simmons, D. A. Ritchie, A. Cavanna, B. Etienne, G. Martinez, and P. Wyder, Phys. Rev. Lett. **79**, 3238 (1997).
[2]M. A. Wilde, J. I. Springborn, O. Roesler, N. Ruhe, M. P. Schwarz, D. Heitmann, and D. Grundler, Phys. Status Solidi B **245**, 344 (2008).
[3]H. L. Störmer, T. Haavasoja, V. Narayanamurti, A. C. Gossard, and W. Wiegmann, J. Vac. Sci. Technol., B **1**, 423 (1983).
[4]I. Meinel, D. Grundler, D. Heitmann, A. Manolescu, V. Gudmundsson, W. Wegscheider, and M. Bichler, Phys. Rev. B **64**, 121306 (2001).
[5]A. Usher and M. Elliott, J. Phys.: Condens. Matter **21**, 103202 (2009).
[6]A. C. Bleszynski-Jayich, W. E. Shanks, and J. G. E. Harris, Appl. Phys. Lett. **92**, 013123 (2008).
[7]J. Jang, D. G. Ferguson, V. Vakaryuk, R. Budakian, S. B. Chung, P. M. Goldbart, and Y. Maeno, Science **331**, 186 (2011).
[8]J. Jang, R. Budakian, and Y. Maeno, Appl. Phys. Lett. **98**, 132510 (2011).
[9]M. A. Wilde, B. Rupprecht, F. Herzog, A. Ibrahim, and D. Grundler, Phys. Status Solidi B **251**, 1710 (2014).
[10]M. A. Wilde, D. Reuter, C. Heyn, A. D. Wieck, and D. Grundler, Phys. Rev. B **79**, 125330 (2009).
[11]B. Rupprecht, S. Heedt, H. Hardtdegen, T. Schäpers, C. Heyn, M. A. Wilde, and D. Grundler, Phys. Rev. B **87**, 035307 (2013).
[12]Y. Y. Wei, J. Weis, K. v. Klitzing, and K. Eberl, Appl. Phys. Lett. **71**, 2514 (1997).
[13]V. T. Dolgopolov, A. A. Shashkin, A. V. Aristov, D. Schmerek, W. Hansen, J. P. Kotthaus, and M. Holland, Phys. Rev. Lett. **79**, 729 (1997).
[14]J. P. Eisenstein, L. N. Pfeiffer, and K. W. West, Phys. Rev. B **50**, 1760 (1994).
[15]L. H. Ho, L. J. Taskinen, A. P. Micolich, A. R. Hamilton, P. Atkinson, and D. A. Ritchie, Appl. Phys. Lett. **96**, 212102 (2010).
[16]D. Zhang, X. Huang, W. Dietsche, K. von Klitzing, and J. H. Smet, Phys. Rev. Lett. **113**, 076804 (2014).
[17]S. Kim, I. Jo, D. C. Dillen, D. A. Ferrer, B. Fallahazad, Z. Yao, S. K. Banerjee, and E. Tutuc, Phys. Rev. Lett. **108**, 116404 (2012).
[18]K. Lee, B. Fallahazad, J. Xue, D. C. Dillen, K. Kim, T. Taniguchi, K. Watanabe, and E. Tutuc, Science **345**, 58 (2014).
[19]R. Winkler, *Spin-Orbit Coupling Effects in Two-Dimensional Electron and Hole Systems*, Springer Tracts in Modern Physics Vol. 191 (Springer, Berlin, Heidelberg, 2003).
[20]S. Datta and B. Das, Appl. Phys. Lett. **56**, 665 (1990).
[21]J. Schliemann, J. C. Egues, and D. Loss, Phys. Rev. Lett. **90**, 146801 (2003).
[22]J. Nitta, T. Akazaki, H. Takayanagi, and T. Enoki, Phys. Rev. Lett. **78**, 1335 (1997).
[23]D. Grundler, Phys. Rev. Lett. **84**, 6074 (2000).
[24]P. Miro, M. Audiffred, and T. Heine, Chem. Soc. Rev. **43**, 6537 (2014).
[25]H. Hardtdegen, R. Meyer, M. Hollfelder, T. Schäpers, J. Appenzeller, H. Løken-Larsen, T. Klocke, C. Dieker, B. Lengeler, H. Lüth, and W. Jäger, J. Appl. Phys. **73**, 4489 (1993).
[26]N. Ruhe, J. I. Springborn, C. Heyn, M. A. Wilde, and D. Grundler, Phys. Rev. B **74**, 235326 (2006).
[27]J. I. Springborn, N. Ruhe, C. Heyn, M. A. Wilde, D. Heitmann, and D. Grundler, Physica E **34**, 172 (2006).
[28]B. Das, S. Datta, and R. Reifenberger, Phys. Rev. B **41**, 8278 (1990).
[29]J. Knobbe, "Rashba-Effekt in niedrigdimensionalen InGaAs/InP Strukturen", Ph.D. thesis (RWTH Aachen, 2004).
[30]T. Schäpers, G. Engels, J. Lange, T. Klocke, M. Hollfelder, and H. Lüth, J. Appl. Phys. **83**, 4324 (1998).
[31]D. Zhang, J. Phys. A: Math. Gen. **39**, L477 (2006).
[32]M. A. Wilde and D. Grundler, New J. Phys. **15**, 115013 (2013).
[33]A. H. MacDonald, H. C. A. Oji, and K. L. Liu, Phys. Rev. B **34**, 2681 (1986).